Science and Technology Indonesia
e-ISSN:2580-4391 *p*-ISSN:2580-4405
Vol. 9, No. 3, July 2024

Research Paper

Synthesis of Silver Nitrate by Evaporation Chemical Reduction Process as Potential Materials for Silver Nanowires Application

Junaidi[1,2]*, Daffa Abdul Malik[1], Muhammad Rizki[1], Indah Pratiwi[1], Pulung Karo-Karo[1], Roniyus Marjunus[1], Dwi Asmi[1], Sutopo Hadi[3]

[1]*Department of Physics, Faculty of Mathematics and Natural Sciences, Universitas Lampung, Bandar Lampung, 35145, Indonesia*
[2]*Materials Research Group, Department of Physics, Universitas Lampung, Bandar Lampung, 35145, Indonesia*
[3]*Department of Chemistry, Faculty of Mathematics and Natural Sciences, Universitas Lampung, Bandar Lampung, 35145, Indonesia*
***Corresponding author**: junaidi.1982@fmipa.unila.ac.id

Abstract
In this study, we conducted the extraction of silver nitrate ($AgNO_3$) using the chemical reduction evaporation method, involving silver metal (Ag) with a molarity of 7.716 M and nitric acid (HNO_3). The heating process via evaporation was carried out at 85 °C for 2 hours. Subsequently, the synthesis of silver nanowires (AgNWs) was performed using a 0.3 M of $AgNO_3$ solution in ethylene glycol (EG), polyvinyl pyrrolidone (PVP), and Iron (III) Chloride hexahydrate ($FeCl_36H_2O$). XRD analysis of the $AgNO_3$ sample revealed an orthorhombic crystal structure with a single $AgNO_3$ phase peak. In AgNWs, three crystalline phases were observed, with the Ag phase being the most dominant. The average crystal size of $AgNO_3$ and AgNWs was 109.42 nm and 22.06 nm, respectively. The average crystal size of the $AgNO_3$ sample may be influenced by the aggregation between crystal nuclei during the heating process. XRF analysis indicated a 98.84% Ag concentration in $AgNO_3$. SEM-EDS analysis showed that the $AgNO_3$ sample had a non-aggregated morphological structure, with particle size measuring 49.46 μm and an overall $AgNO_3$ purity of 92.68%. The SEM image of the AgNWs sample displayed a very homogeneous diameter of ~200 nm with a length of around 10-20 μm. Meanwhile, AgNWs exhibited a morphology resembling rod-shaped wires with a purity of 68% for Ag.

Keywords
Silver Nitrate, Silver Nanowires, Polyol, Evaporation, Characterization

Received: 20 March 2024, Accepted: 18 May 2024
https://doi.org/10.26554/sti.2024.9.3.642-650

1. INTRODUCTION

One of the elements that occurs naturally in the earth's crust is metal; it is estimated that the amount of metal in the earth's crust is 4%; some examples of metals that can be found include ruthenium (Ru), rhodium (Rh), palladium (Pd), silver (Ag), osmium (Os), iridium (Ir), platinum (Pt), and gold (Au). Metals have good heat conductor properties and are malleable, strong, and corrosion-resistant, so some metals are expensive. Among several metals, we can find that silver is a metal in great demand by the public. Silver is a white, shiny, soft metal and can be forged using electricity and high temperatures. Silver has an advantage over other metals, namely that it can melt with other metals. Silver is even used as a substitute for tin because silver does not cause environmental pollution. Silver has low resistance to electric current, so it is also widely used as a material for making electrical tools. Silver is also an element that can absorb and conduct heat well; silver has a long-lasting color unless exposed to air pollution. Silver also has a relatively lower price than gold, and silver has high electrical and thermal conductivity compared to other metals; silver is also easier to find than other metals (Robinson et al., 2022).

Several chemicals can be made from silver as the main ingredient, such as silver nitrate ($AgNO_3$), silver chloride (AgCl), silver sulfide (Ag_2S), and silver oxide (Ag_2O). Silver nitrate is a compound formed from silver and nitric acid (HNO_3). Silver nitrate has several advantages over other compounds, such as its usefulness as a precursor for other silver compounds. Apart from that, the advantage of the silver nitrate compound is that it is relatively stable to light and can dissolve in many solvents, such as water, compared to the silver chloride compound, which is difficult to dissolve in water. The silver nitrate compound is also less sensitive to sunlight than silver sulfide, a compound resulting from a combination of silver and sulfur (S) which has sensitive properties to sunlight (Asif et al., 2022; Kim et al., 2024).

With time, using silver nitrate compounds in various sectors has become essential for Indonesian society. These sectors include industry, electronics, photography, healthcare, and the environment. The utilization of the compound $AgNO_3$ can

be achieved through the development of silver nanoparticle technology. Silver nanoparticles (AgNPs) obtained from the synthesis of $AgNO_3$ with a purity percentage of 99.99% are highly effective in reducing toxicity effects and serve as antimicrobial disinfectant agents. In addition, silver nanoparticles can be utilized for water disinfection in the environmental preservation sector and can be used as a coating on solar panels to produce excellent photocatalysts (Agrawal et al., 2018; Zaman et al., 2022; Imran et al., 2020).

Furthermore, silver nanoparticles obtained through the synthesis of $AgNO_3$ with a purity of 99.99% are highly effective as pigments in liquid crystal display (LCD) screens to produce high-quality and vibrant red-green-blue (RGB) displays. The decline in screen quality can occur by replacing the material indium thin oxide (ITO) with silver nanowires (AgNWs) because of ITO's high resistance level on LCD screens. High resistance levels can increase noise or distortion in electrical signals and produce less accurate colors, thus lowering image quality. To enhance image quality, ITO can be replaced with AgNWs. AgNWs can reduce resistance levels by up to 29.5%, reaching 24.1 Ω/sq with a transmittance level of 96.4%. Therefore, the time gap in the displayed colors on the screen becomes shorter and more accurate. Additionally, if a conductive layer with low resistance is used on a flexible LCD screen, it can enhance durability and flexibility. Low resistance on flexible substrates helps reduce the risk of damage or cracks during flexibility (Abdali et al., 2023).

This is the reason for the high price of $AgNO_3$ powder with a purity greater than 99%. Factors that can affect the purity level of $AgNO_3$ include impurity elements, such as plumbum (Tb), gold (Au), copper (Cu), and other impurities in silver. To achieve a high purity level, the purity percentage of silver metal used must be above 99%, and nitric acid (HNO_3) must be above 68% (Menamparambath et al., 2015; Badán et al., 2020). As a result, very few scientists are interested in experimenting with this silver nitrate synthesis. Previous research on $AgNO_3$ has observed the influence of the optimal mass percentage of Ag by identifying the kinetic rate of a chemical reaction in terms of heating time and temperature. This testing employed the chemical reduction evaporation method with a heating temperature of 85 °C. The study involved varying the heating times at 15 s, 45 s, and 120 s. The results obtained indicated that Ag could crystallize within 120 s. A limitation of this study is that it did not examine the crystal structure and particles through X-ray diffraction (XRD,) X-ray fluorescence (XRF), and Scanning Electron Microscope-Energy Dispersive X-Ray (SEM-EDX) characterizations (Özmetin et al., 2001). Other research has also utilized the evaporation method with a molar ratio 1:1.5 between Ag and HNO_3. The XRF analysis results revealed the presence of trace impurity elements in the $AgNO_3$ sample prepared, amounting to less than 0.002 part per million (ppm). This indicates a very high level of purity for $AgNO_3$ in this study (Habashi and Sora, 1997).

Based on previous research, this research will synthesize AgNWs using $AgNO_3$ obtained from prior studies. The synthesis of $AgNO_3$ involves the chemical evaporation method, employing Ag and HNO_3. Subsequently, the synthesis of AgNWs is carried out based on the polyol method, utilizing $AgNO_3$ (from the preceding synthesis), Polyvinylpyrrolidone (PVP), Iron (III) Chloride Hexahydrate ($FeCl_3{\cdot}6H_2O$), and ethylene glycol (EG) as a solvent. The samples of $AgNO_3$ and AgNWs are then characterized to observe their crystal properties, morphology, and size through XRD, XRF, and SEM-EDX. The results of this synthesis have the potential for applications in various technological fields that utilize the unique properties of AgNWs, such as the production of nanoscale sensors, more efficient optoelectronic devices, and more. By continuously developing nanowires (NWs) synthesis techniques, we can open opportunities for innovation in the future (Mozammel et al., 2006; Giri et al., 2022).

2. EXPERIMENTAL SECTION

2.1 Materials

For synthesis $AgNO_3$ the material used silver metal granules (ANTAM with 99%), solution nitric acid (HNO_3) (Sigma-Aldrich Pte. Ltd with 68%), and deionized water. The materials used for synthesis AgNWs were silver nitrate ($AgNO_3$) resulting from synthesis, polyvinyl pyrrolidone (PVP Mw. 55,000 g/mol, Sigma-Aldrich Pte. Ltd.), ethylene glycol (EG 99.5%, Merck kGaA, Darmstadt, Germany), ethanol 96% (Merck kGaA, Darmstadt, Germany), iron (III) chloride hexahydrate ($FeCl_3{\cdot}6H_2O$, Sigma-Aldrich Pte. Ltd.), silicon oil, and deionized water.

2.2 Methods

Synthesis of $AgNO_3$; the sample extraction process commenced by mixing 10 grams of silver metal with 12 mL of HNO_3 solution. Afterward, the mixture was heated at 85 °C for 2 hours. Then, the sample was cooled until its temperature decreased, as shown in Figure 1a. The crystallization process begins by drying the sample, which still contains a significant amount of water, in an oven at a heating temperature of 125 °C for 10 minutes. Subsequently, the dried $AgNO_3$ crystals are weighed using an analytical balance with repetitions carried out four times.

Synthesis of AgNWs; AgNWs were obtained using the polyol method, with PVP as a reducing agent and ethylene glycol (EG) as a solvent. The $AgNO_3$ solution is prepared with a concentration of 0.3 M in 40 mL of EG. Meanwhile, the $FeCl_3{\cdot}6H_2O$ solution is prepared with a concentration of 0.1 M in 10 mL of EG. The dissolution process in the EG solution is carried out at room temperature and stirred for ±10 minutes until completely dissolved. The solution is then stored in a container for the next stage of the process. Next, 0.45 M of PVP is placed in an Erlenmeyer flask and dissolved in 100 mL of EG. In the first step in the synthesis of AgNWs, 4.995 g of PVP was dissolved in 100 mL of EG using an Erlenmeyer flask and stirred at 140 °C for 20 minutes. Then, a $FeCl_3{\cdot}6H_2O$/EG 0.25 mL solution was injected using a syringe for ±5 minutes. Next, an amount of 40 mL of the $AgNO_3$/EG was dripped

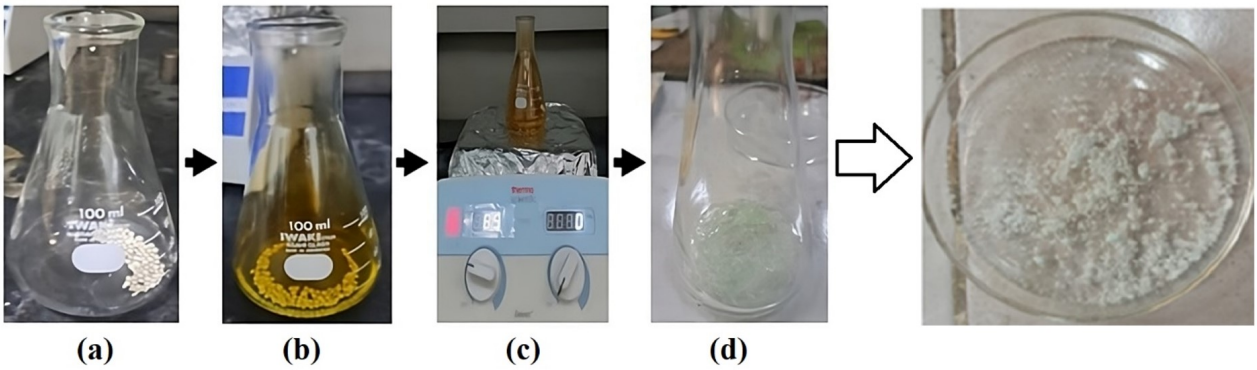

Figure 1. Results from the Evaporation Process

using a burette for ±30 minutes. After that, the solution is stirred for ±2 hours until it changes color to silver-gray. Finally, the AgNWs solution was cooled at ambient temperature and centrifuged at 3000 rpm for 10 minutes, repeated three times to remove any remaining solvent and other impurities. The AgNWs colloid was stored in ethanol for characterization (Junaidi et al., 2021).

2.3 Characterization

The characterization of the $AgNO_3$ sample includes XRD, XRF, SEM, and EDX analyses. The XRD characterization was conducted using the D8 Advance instrument. This process is carried out to analyze the phase peaks formed and the average crystal size. The analysis includes both qualitative and quantitative aspects. To perform this process, the sample must be in powder form. The XRD graph range spans from 2θ at 10-90°. The crystal structure of AgNWs was analyzed with (Shimadzu R6000) by CuKα (λ = 1.54184 Å) with a scanning 2θ in the range of 20° to 90°. XRF characterization was carried out using the Omnian ED XRF PANalytical Epsilon instrument. This process measures the total percentage concentration of elements in the sample. The $AgNO_3$ sample must have a mass of more than 3 grams. The results obtained from XRF analysis include the percentage concentration of elements presented in percentages (%) and parts per million (ppm). The SEM-EDX characterization was observed using scanning electron microscopy (JEOL, JSM-6510) by accelerating a voltage of 10 kV. The EDX analysis determines the total mass percentage of elements such as Ag, N, O, and other impurity elements.

3. RESULTS AND DISCUSSIONS

The results of the evaporation method on Ag metal and HNO_3 (68%) at 85 °C for 2 hours are shown in Figure 1. Silver metal will slowly begin to react with HNO_3 as shown in Figure 1(a). After 10 minutes, the sample starts changing to yellowish and emitting transparent black smoke. Figure 1(b) shows the process can occur due to the release of nitrogen dioxide (NO_2) gas into the air, and the chemical reaction rate is prolonged. The sample will turn into a deep yellow color and emit black smoke as shown in Figure 1(c). Figure 1(d) shows the resulting $AgNO_3$ precipitate, which will be dried using an oven at 125 °C.

The results of the crystallization process for $AgNO_3$ indicate that the particle size of the sample starts to shrink and transform into a powder. The obtained $AgNO_3$ sample appears bluish-white. This is influenced by the tiny mass of Ag during the chemical reaction. If the Ag mass is lower, it increases the likelihood of chemical reactions between HNO_3 and elements other than Ag, such as Cu. Cu more readily reacts with HNO_3, forming $Cu(NO_3)_2$ and occupying vacant spaces, displacing Ag. This is influenced by the fact that Cu is more reactive compared to Ag. The more $Cu(NO_3)_2$ occupies the vacant spaces, the more intense the blue color becomes (Sembiring et al., 2022; Junaidi et al., 2022).

The resulting $AgNO_3$ samples were used for the synthesis of AgNWs. The synthesis of AgNWs begins with dissolving PVP/EG and adding $FeCl_3{\cdot}6H_2O$/EG solution. After the $AgNO_3$/EG solution was injected into the PVP/EG and $FeCl_3{\cdot}6H_2O$/EG solutions, the color of the solution slowly changed to brownish. This indicates that reducing Ag^+ ions to Ag atoms is occurring. After ±1 hour, the solution changed to pale yellow, indicating the formation of silver nanoparticles (AgNPs) formation. After being synthesized for ±2 hours, the color of the solution will change to gray, approaching white, which indicates that AgNWs have been formed. After being synthesized for ±2 hours, all the AgNPs formed were capped and turned into AgNWs. The AgNWs colloidal sample's final result greatly influences the Ag nanostructure's geometric shape formed in the AgNPs formation process (Junaidi et al., 2022; Khan, 2018).

3.1 X-ray Fluoresences Analysis

The results of the XRF characterization of the silver metal used in the silver granule preparation stage. The elemental composition of the samples is detailed below. Silver (Ag) is the predominant element, constituting approximately 98.07% of the composition. Other detected elements include phosphorus (P) at 0.21%, copper (Cu) at 1.08%, calcium (Ca) at 0.49%, and zirconium (Zr) at 0.15%. Additionally, trace amounts of silicon (Si) were found at 265.0 parts per million (ppm),

iron (Fe) at 383.5 ppm, zinc (Zn) at 218.8 ppm, and gold (Au) at 440.9 ppm. These findings provide a comprehensive overview of the elemental distribution in the analyzed silver metal granules. The total percentage concentration from silver granules is 98,07%. Compared to the minimum standard, the purity of silver does not meet the criteria for good pure silver (less than 99.95%) (Hennenkamp et al., 1994). Several factors influence the presence of impurity elements, stemming from the inherent source of the silver metal and the lack of cleanliness within the laboratory.

Furthermore, the XRF analysis results of the $AgNO_3$ show the sample's elemental composition, which is outlined as follows: silver (Ag) dominates the composition with a concentration of 98.84%. Calcium (Ca) and copper (Cu) are in smaller amounts at 0.494% and 0.412%, respectively. Additionally, trace elements include phosphorus (P) at 0.213 parts per million (ppm), silicon (Si) at 172.2 ppm, titanium (Ti) at 48.50 ppm, bromine (Br) at 28.90 ppm, terbium (Tb) at 25.00 ppm, osmium (Os) at 18.90 ppm, and gold (Au) at 136.2 ppm. These findings offer a comprehensive insight into the elemental distribution within the analyzed $AgNO_3$ sample. XRF data also indicates an increase in the concentrations of Cu and Ca by 0.412% and 0.494%, respectively. The increase in Cu concentration is influenced by the highly reactive nature of Cu when it reacts with HNO_3 (Krishnamurthy, 1977; Mamuru and Happy, 2018). This demonstrates the binding of impurity elements with the $AgNO_3$ sample, which is why the sample appears bluish-white. This indicates that the amount of impurity elements is very small. However, it significantly affects the phase produced by the $AgNO_3$ compound.

3.2 X-ray Diffraction Analysis

Figure 2 shows the results of the qualitative analysis from the XRD characterization process from AgNWs and $AgNO_3$. The results indicate the presence of several crystal phase peaks from AgNWs, such as a is silver (Ag), b is silver diammine nitrate ($Ag(NH_3)_3NO_3$), and c is hematite (Fe_2O_3). Meanwhile, in the $AgNO_3$ graph, there are several phases such as d is silver nitrate ($AgNO_3$), e is silver dinitramide (AgN_3O_4), f is silver nitrite ($AgNO_2$), g is silver oxide (Ag_2O), h is calcium nitrate ($Ca(NO_3)_2$), i is copper nitrate ($Cu(NO_3)_2$), and j is silver phosphate (Ag_3PO_4).

Figure 2 also shows AgNWs graph shows the X-ray diffraction pattern with diffraction peaks at 2θ angles of 37.58°, 43.77°, 63.98°, 76.96°, and 81.11°. These diffraction angles correspond to the crystal planes of AgNWs with Miller indices (111), (200), (220), (311), and (222), with a face-centered cubic (fcc) crystal structure. The high diffraction peaks indicate that the formed AgNWs have a high level of crystallinity. In addition to the diffraction peaks of AgNWs, the diffractogram also shows other peaks at 2θ angles of 33.75°, 39.28°, 57.07°, and 68.26°. The graph indicates that these peaks are impurities in the sample. However, overall, the produced AgNWs sample is quite good, with a purity level reaching 61.1%.

According to the graph in Figure 2, 29 crystal peaks are present in $AgNO_3$, which arise from 7 different phases apart from the $AgNO_3$ phase. The $AgNO_3$ phase itself appears in 5 peaks on the diffraction angle (21.89°, 24.51°, 53.33°, 66.67°, and 78.38°). On the other hand, the AgN_3O_4 phase shows 14 peaks on this graph. Therefore, the AgN_3O_4 phase becomes the most dominant crystal phase in the sample of $AgNO_3$. The $AgNO_3$ graph shows that using a volume of 12 mL of HNO_3 with 10 grams of Ag metal causes the bonds between atoms to become unstable and may lead to new phases other than $AgNO_3$. As the mole ratio approaches its stable level, the bonds become more stable (Htwe et al., 2019; Evans and Evans, 2021). Meanwhile, the quantitative analysis result from AgNWs and $AgNO_3$ with XRD characterization are shown in Figure 3.

Figure 3 shows the results from $AgNO_3$ and AgNWs analysis. Figure 3(a) shows the molar percentage results from the analysis of $AgNO_3$ and presents the distribution of various phases in the sample. The predominant phase is AgN_3O_4, constituting 42.81% of the composition, followed by $AgNO_3$ at 27.31%. Other identified phases include $Ca(NO_3)_2$ at 11.69%, $Cu(NO_3)_2$ at 12.33%, and Ag_3PO_4 at 2.95%. Additionally, minor contributions are observed from $AgNO_2$ at 1.54% and Ag_2O at 1.39%. These molar percentages provide valuable insights into the molecular composition and phase distribution within the $AgNO_3$ sample. The refinement output data yields a profile residual (R_p) value of 9.09%, a weighted profile residual (R_wp) of 10.80%, and a Goodness of Fit (GOF) value of 0.092%. AgN_3O_4 holds the largest molar percentage at 42.81%. $AgNO_3$ has the second-highest molar percentage at 27.31%. $Cu(NO_3)_2$ has the third-highest molar percentage at 12.33%. This indicates that AgN_3O_4 has the highest molar percentage. The lattice parameters of the $AgNO_3$ phase are a = 6.9264 Å, b = 7.3400 Å, and c = 9.9922 Å. The analysis results are acceptable if the R_p and R_wp output values are less than 20%, and a GOF is less than 4% (Khan, 2018; Hennenkamp et al., 1994). These results indicate that lattice structures shift compared to COD as shown in Table 1.

Table 1. Results of the Refinement from $AgNO_3$

Phase	a(Å)	b(Å)	c(Å)	a(°)	b(°)	c(°)
$AgNO_3$	6.9264	7.3400	9.9922	90	90	90
AgN_3O_4	5.8101	9.8957	14.1490	90	90	90
$AgNO_2$	3.6843	6.2946	5.0235	90	90	90
Ag_2O	4.8476	4.8476	4.8476	90	90	90
Ag_3PO_4	6.0726	6.0726	6.0726	90	90	90
$Cu(NO_3)_2$	10.189	5.0541	8.3211	90	90	90
$Ca(NO_3)_2$	7.6750	7.6750	7.6750	90	90	90

Figure 3(b) is the molar percentage results for AgNWs outlined in Table 2, delineating the composition of various phases within the sample. The primary phase identified is $Ag(NH_3)_3NO_4$, comprising 50.68% of the composition, followed by Fe_2O_3 at 38.76%. Additionally, a more minor con-

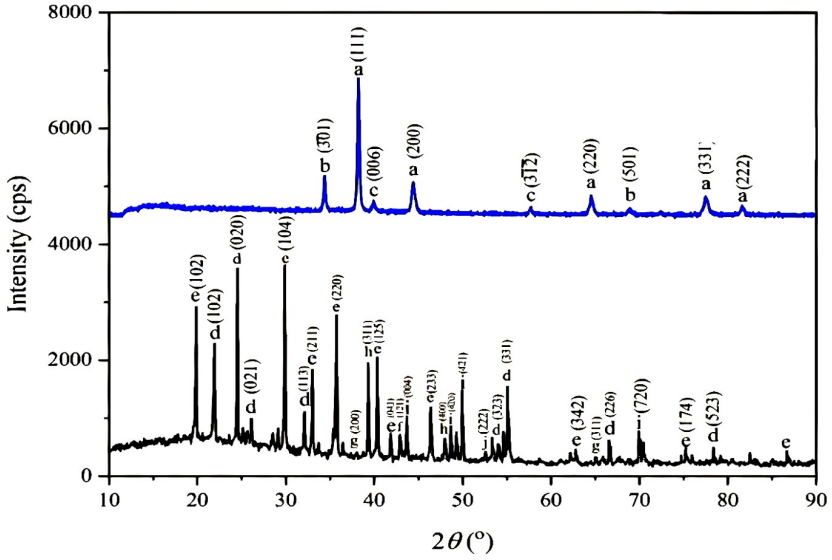

Figure 2. XRD Pattern of (a) $AgNO_3$ and (b) AgNWs

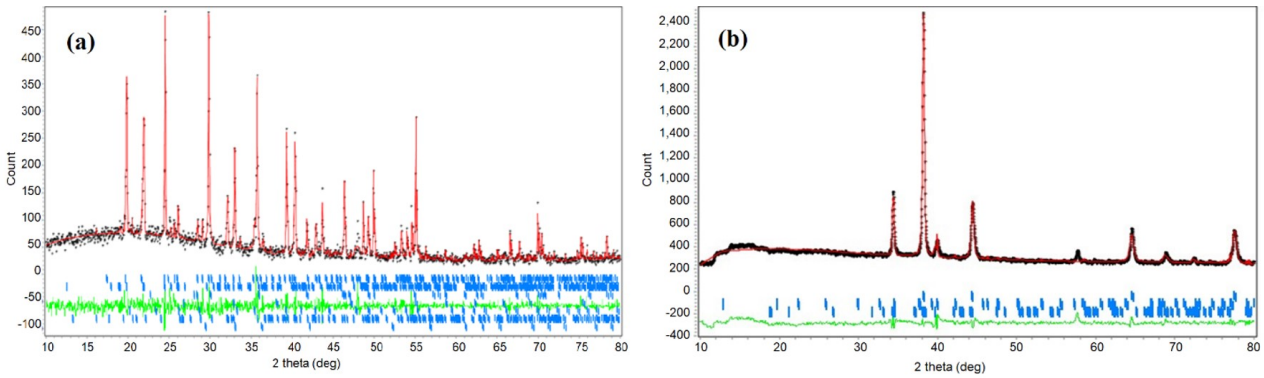

Figure 3. Refinement Results from Quantitative Analysis of (a) $AgNO_3$ and (b) AgNWs

tribution is observed from elemental Ag at 10.56%. These findings shed light on the molecular distribution of phases in the AgNWs, with a predominant presence of $Ag(NH_3)_3NO_4$ and significant proportions of Fe_2O_3, providing valuable insights into the material's composition. The refinement output data yields an R_p value of 3,56%, a weighted R_wp of 4,87%, and a GOF value of 0,79%. $Ag(NH_3)_3NO_4$ holds the most significant molar percentage at 50,68%. Fe_2O_3 has the second-highest molar percentage at 38.76%. Ag has the third-highest molar percentage at 10.56%. These results indicate that lattices shift compared to COD as shown in Table 2.

Table 2. Results of the Refinement from AgNWs

Phase	a (Å)	b (Å)	c (Å)	a(°)	b(°)	c(°)
Ag	4.08096	4.08096	4.08096	90	90	90
$Ag(NH_3)_3NO_4$	7.94369	7.94369	5.97147	90	90	90
Fe_2O_3	2.82189	9.36284	9.44719	90	90	90

Table 2 indicates that the lattice parameters for Ag are a = 4.08096, b = 4.08096, and c = 4.08096. These results suggest a shift in the lattice parameters compared to the database indices. This may be influenced by impurity content in the AgNWs sample. The presence of Fe_2O_3 and $Ag(NH_3)_3NO_4$ indicates the existence of impurities that reduce the purity of the silver itself. The average crystal size can be obtained from XRD diffractograms, and the data obtained can be used to determine the crystal size using the full width at half-maximum (FWHM). The crystal size is obtained from the Debye-Scherrer equation as shown in Equation (1).

$$D = \frac{k\lambda}{(\beta \cos\theta)} \quad (1)$$

with D as the crystal size, K as a factor (0.9), λ as the wavelength of X-rays, β as the value of FWHM, and θ as the diffraction angle. This measurement uses the origin-lab to measure FWHM values at the highest peaks of each formed phase (Mamuru and

Happy, 2018). The results are presented in Table 3 and Table 4.

Table 3. Crystal Size Calculation from $AgNO_3$

Phase	2θ (°)	FWHM (nm)	Crystal Size (nm)
$AgNO_3$	24.51	0.064	124.06
AgN_3O_4	29.87	0.093	87.62
$AgNO_2$	42.86	0.116	70.99
Ag_2O	38.72	0.060	138.86
$Ca(NO_3)_2$	39.32	0.062	132.59
$Cu(NO_3)_2$	49.95	0.094	91.02
Ag_3PO_4	53.98	0.072	120.88

Table 4. Crystal Size Calculation from AgNWs

Phase	2θ (nm)	FWHM (nm)	Crystal Size (nm)
Ag	38.21	0.254	33.09
$Ag(NH_3)_3NO_4$	34.39	0.255	32.62
Fe_2O_3	59.69	19.19	0.48

The average crystal size result from $AgNO_3$ is 109.42 nm, which is smaller than the previous research, which was 112 nm (Htwe et al., 2019). The average crystal size of the $AgNO_3$ sample can be influenced by the aggregation between crystal nuclei during the heating process. The average crystal size of AgNWs is 22.06 nm, which is quite different from previous research that obtained an average crystal size of 30.90 nm (Siddiqui et al., 2023; Lakshmi, 2016; Ha et al., 2022).

3.3 SEM-EDX Analysis

The SEM characterization process aims to determine the morphology of particles in the $AgNO_3$ and AgNWs samples, the average particle size, and the mass percentage of the constituent elements of the $AgNO_3$ and AgNWs samples. The SEM analysis results for the $AgNO_3$ sample and AgNWs are shown in Figure 4.

Figures 4(a) and 4(b) depicts the morphological structure of the $AgNO_3$, which indicates that the particles do not agglomerate and have very small sizes. The particles have a bright overall color, indicating a very high metal content (Cao et al., 2020; Villalpando et al., 2020). The average particle size obtained is 49.46 μm. This result is significantly different from the latest research, which reported average $AgNO_3$ particle sizes ranging from 200 to 600 μm. Figures 4(c) and 4(d) shows that the morphology of AgNWs colloids is influenced by several factors, such as the heating process, injection rate, and time for AgNWs synthesized. During the process of dissolving PVP/EG and adding the $FeCl_3.6H_2O$/EG solution, a clear solution was obtained and did not change color. After the $AgNO_3$/EG solution was injected into the PVP/EG and $FeCl_3.6H_2O$/EG solutions, the color of the solution slowly changed to brownish. This indicates that reducing Ag^+ ions to Ag atoms is occurring. After ±1 hour, the solution changed color to pale yellow, indicating the formation of silver nanoparticles (AgNPs). After being synthesized for ±2 hours, the color of the solution will change to gray, approaching white, which indicates that silver nanowires or silver nanowires (AgNWs) have been formed. AgNWs have a remarkably uniform diameter measuring $(2.0 \pm 1) \times 10^2$ nm, coupled with a length of approximately $(8 \pm 2) \times 10^4$ nm. These findings indicate that the resulting AgNWs have an exceptionally elongated size compared to various existing research results on AgNWs (Liu et al., 2020). The mass percentage analysis for both $AgNO_3$ and AgNWs provides insights into the respective samples' elemental composition. In the $AgNO_3$ sample, silver (Ag) constitutes 55.55% of the mass, followed by oxygen (O) at 28.47%, and nitrogen (N) at 8.32%. Trace elements such as copper (Cu), calcium (Ca), and gold (Au) are present in smaller percentages. Conversely, in the AgNWs sample, silver (Ag) dominates with a mass percentage of 71.24%, oxygen (O) at 17.60%, carbon (C) at .91%, and iron (Fe) at 3.25 also contribute to the composition, though in smaller proportions. These mass percentage values provide a comprehensive understanding of the elemental distribution in both $AgNO_3$ and AgNWs, highlighting the significant differences in their compositions. This can be explained by impurity elements within the silver material, as highlighted in the XRF analysis results (?). As a result, it reduces the purity level of the produced $AgNO_3$. The total purity of the $AgNO_3$ sample is 92.68%. Meanwhile, the AgNWs sample has a total purity percentage of 67%, with the remainder comprising impurity elements present in the AgNWs sample. These results indicate that silver (Ag) has the highest count in both samples, suggesting its dominance. This provides evidence that silver nanowires have formed.

3.4 TEM Analysis

The characterization process using TEM was carried out to see the surface morphology and geometry and determine the crystal structure of the AgNWs colloid. This characterization will obtain sample morphology and diffraction ring patterns representing the crystal planes formed. The diffraction ring analysis process uses lattice parameter data from XRD diffraction analysis calculations. These results were compared with the XRD analysis results to determine the crystal structure of the AgNWs colloid. The TEM analysis results of AgNWs are shown in Figure 5.

In addition, from the results of characterization using TEM, diffraction ring patterns of AgNWs will be obtained, which will determine the crystal planes of AgNWs. The diffraction ring pattern was then analyzed using ImageJ software to calculate the distance of each diffraction ring from the center of the circle. The diffraction data will later be compared with the diffraction data from the test results using XRD so that the results obtained can be strengthened from the XRD results. To find out the crystal planes of the diffraction ring, it can be obtained using Equations (2) and (3).

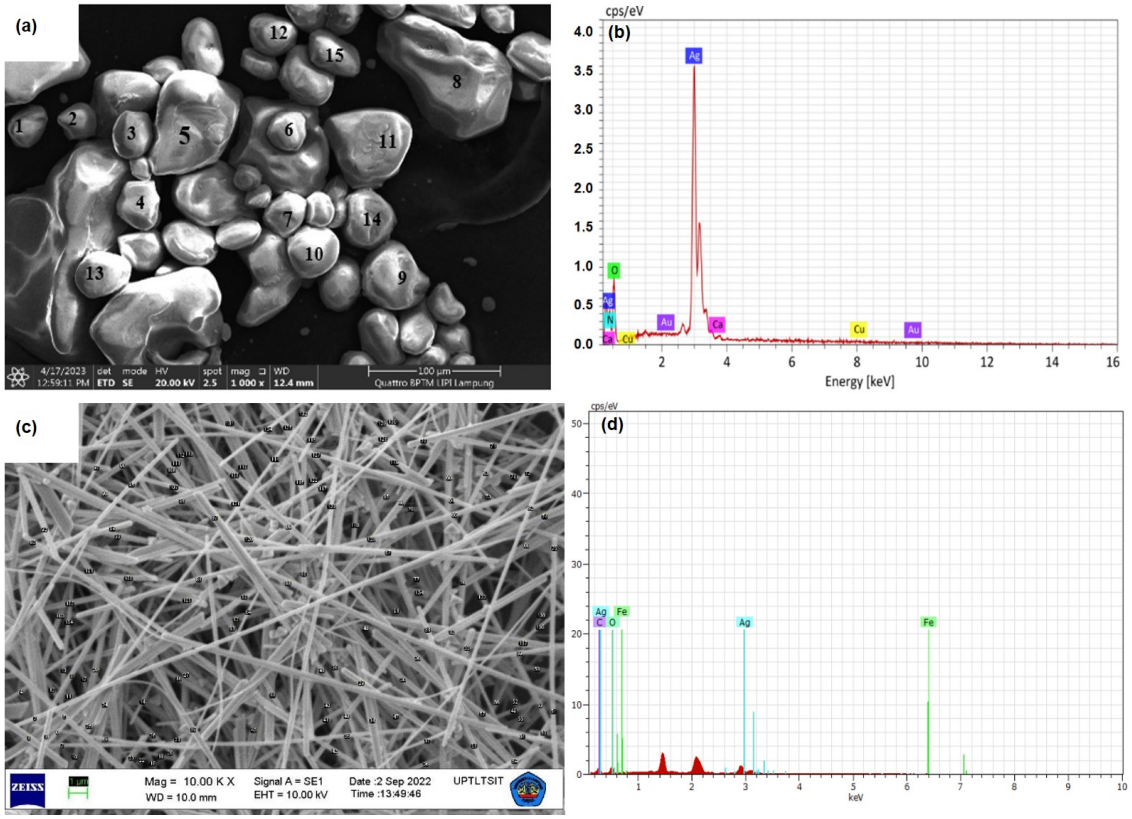

Figure 4. SEM-EDS Images from Sample of (a-b) $AgNO_3$ and (c-d) AgNWs

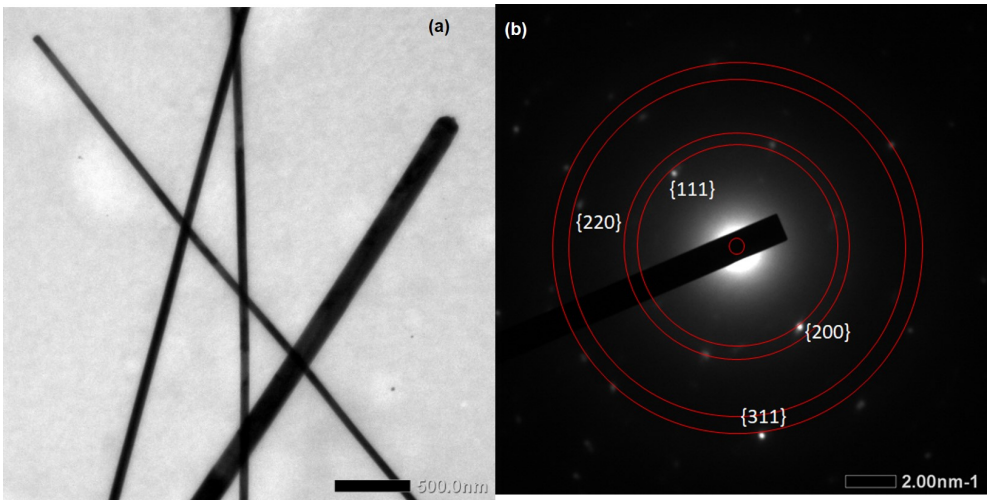

Figure 5. TEM Images of AgNWs (a) and SAED of AgNWs (b).

$$R\,d = \lambda L, \tag{2}$$

$$d^2 = \frac{a^2}{\sqrt{h^2 + k^2 + l^2}}, \tag{3}$$

where R is the distance of the diffraction ring from the center of the circle, d is the distance between the Bragg planes, λ is the wavelength used in TEM, L is the lens distance, a is the grating constant, and h, k, l are the Miller indices as shown in Table 5.

From the morphology in Figure 5(a), the diameter of Ag-NWs is around 60-200 nm. In Figure 5(a), we can also see the

Table 5. Miller Index of AgNWs Colloidal Samples

R (nm)	λ ($\times 10^{-3}$ nm)	L (nm)	d (nm)	a (nm)	$h^2+k^2+l^2$	Miller Index (hkl)
3.893	3.35	284.29	0.245	0.4142	2.85	111
4.294	3.35	284.29	0.222	0.4142	3.490	200
6.549	3.35	284.29	0.145	0.4142	8.143	220
7.468	3.35	284.29	0.128	0.4142	10.688	311

tip morphology of the AgNWs, which shows a geometry that resembles the pentagonal cross-section of decahedral particles. As is known in theory, decahedral particles, often called multi-twin particles (MTPs), have five planes of symmetry with a surface of 10 planes (111). This plane acts as the growth point of the AgNWs. When decahedral AgNPs are formed, other reduced Ag atoms will form crystallization on the surface of the (111) plane because they have high surface energy. This is what will result in the growth of decahedral AgNPs into AgNWs. At the beginning of formation, the PVP interacts more strongly on the (100) plane than on the (111) plane, so there will be continued growth at both ends of the AgNWs. Because the double plane of the decahedral does not bend during the growth process, AgNWs with a pentagonal cross-section will be formed, which have four planes of symmetry at the ends and surfaces (Zhang and Engholm, 2018; Honey et al., 2022; Wiley et al., 2005). The results of measurements and calculations on the diffraction rings are presented in Table 5.

The calculation results show that all diffraction rings are indexed in the fcc form with Miller index values of around 3.893, 4.294, 6.549, and 7.468. The Miller index corresponds to the fcc crystal structure in the (111), (200), (220), and (311) planes. The crystal structure of AgNWs measured by XRD at a 2θ angle of 20-90° produces four diffraction peaks, namely (111), (200), (220), and (311). This condition proves the AgNWs crystal structure analysis between TEM and XRD is suitable (De Yoreo, 2002; Xia et al., 2009).

Meanwhile, from the analysis of the diffraction ring pattern of the AgNWs colloidal sample as in Figure 4(d), four crystal planes were obtained, namely (111), (200), (220), and (311). From the diffraction ring pattern of the AgNWs, no diffraction ring pattern was formed for the (222) crystal plane, as obtained from the results of the X-ray diffractogram of the AgNWs colloid as shown in Figure 4(a). If we look at the X-ray diffractogram data from the colloidal AgNWs, it shows that the intensity for the (222) plane is smaller than for the other planes, so this makes it possible for the diffraction ring pattern for these two planes not to be seen clearly.

4. CONCLUSIONS

The synthesized $AgNO_3$ demonstrates applicability in nanowire synthesis, indicating a promising prospect for its utilization in various applications. However, it is noteworthy that the purity level of the produced $AgNO_3$ should be further enhanced to achieve optimal performance. The refinement is essential to ensure that silver (Ag) stands out as the sole and dominant element, minimizing the presence of impurities. This enhancement in purity is crucial for maximizing the effectiveness of $AgNO_3$ in nanowire synthesis, thereby improving the overall quality and functionality of the synthesized material. In the XRD analysis, the sample exhibits six peaks in addition to the $AgNO_3$ phase, indicating significant impurities. Meanwhile, in AgNWs, three crystalline phases have formed, with the Ag phase being the most dominant. In the XRF analysis, the sample has an Ag concentration percentage of 98.84% and a Cu concentration of 0.412%. These particles do not agglomerate, have an average particle size of 49.46 μm, and a total mass percentage of 92.68%.

5. ACKNOWLEDGMENT

This work was supported by a research grant of Fundamental Research, Contract No. 131/E5/PG.02.00.PL/2023 by the Ministry of Research, Technology and Higher Education of the Republic of Indonesia via the Institute for Research and Community Services of Universitas Lampung by contract No. 2624/UN26.21/PN/2023.

REFERENCES

Abdali, K., E. Al-Bermany, and K. H. Abass (2023). Impact The Silver Nanoparticles on Properties of New Fabricated Polyvinyl Alcohol- Polyacrylamide- Polyacrylic Acid Nanocomposites Films for Optoelectronics and Radiation Pollution Applications. *Journal of Polymer Research*, **30**(138); 1–19

Agrawal, S., M. Bhatt, S. K. Rai, A. Bhatt, P. Dangwal, and P. K. Agrawal (2018). Silver Nanoparticles and Its Potential Applications: A Review. *Journal of Pharmacognosy and Phytochemistry*, **7**(2); 930–937

Asif, M., R. Yasmin, R. Asif, A. Ambreen, M. Mustafa, and S. Umbreen (2022). Green Synthesis of Silver Nanoparticles (AgNPs), Structural Characterization, and Their Antibacterial Potential. *Dose Response*, **20**(2); 1–11

Badán, J. A., E. Navarrete-Astorga, R. Henríquez, F. Martín, R. E. Marotti, J. R. Ramos-Barrado, and E. A. Dalchiele (2020). Optical Properties of Silver Nanoparticles Deposited onto Silicon Substrates by Different Soft-Solution Processing Techniques. *Optical Materials*, **100**; 109651

Cao, L., Q. Huang, J. Cui, H. Lin, W. Li, Z. Lin, and P. Zhang (2020). Rapid and Facile Synthesis of High-Performance Silver Nanowires by a Halide-Mediated, Modified Polyol

Method for Transparent Conductive Films. *Nanomaterials*, **10**(6); 1139

De Yoreo, J. J. (2002). Principles of Crystal Nucleation and Growth. *Reviews in Mineralogy and Geochemistry*, **54**(1); 57–93

Evans, J. S. O. and I. R. Evans (2021). Structure Analysis from Powder Diffraction Data: Rietveld Refinement in Excel. *Journal of Chemical Education*, **98**(2); 495–505

Giri, A. K., B. Jena, B. Biswal, A. K. Pradhan, M. Arakha, S. Acharya, and L. Acharya (2022). Green Synthesis and Characterization of Silver Nanoparticles Using Eugenia Roxburghii DC. Extract and Activity Against Biofilm-Producing Bacteria. *Scientific Reports*, **12**(1); 8383

Ha, H., C. Amicucci, P. Matteini, and B. Hwang (2022). Mini Review of Synthesis Strategies of Silver Nanowires and Their Applications. *Colloid and Interface Science Communications*, **50**; 100663

Habashi, F. and K. Sora (1997). *Handbook of Extractive Metallurgy*. Wiley

Hennenkamp, J. R., K. M. Logsdon, B. L. Simpson, T. E. Walker, and P. C. Drake (1994). Silver Nitrate Produced by a Continuous Evaporative Crystallization Process. US Patent 5,360,602

Honey, S., H. M. Khan, M. E. Mazhar, J. Ahmad, H. Raza, I. Ahmad, J. Asim, S. Naseem, and M. Maaza (2022). Enhanced Optical Transmittance of Silver Nanowires via Gamma Rays Irradiation. *Journal of King Saud University - Science*, **34**(5); 102058

Htwe, Y. Z. N., W. S. Chow, Y. Suda, and M. Mariatti (2019). Effect of Silver Nitrate Concentration on the Production of Silver Nanoparticles by Green Method. *Materials Today: Proceedings*, **17**; 568–573

Imran, M., C. J. Ehrhardt, M. F. Bertino, M. R. Shah, and V. K. Yadavalli (2020). Chitosan Stabilized Silver Nanoparticles for the Electrochemical Detection of Lipopolysaccharide: A Facile Biosensing Approach for Gram-Negative Bacteria. *Micromachines*, **11**(4); 413–417

Junaidi, L. Afriliani, P. Manurung, S. Sembiring, K. Triyana, and S. Hadi (2022). The Crystal Structure Analysis of Silver Nanowires Using Rietveld Method for Optoelectronic Application. *Journal of Nano Research*, **71**; 1–12

Junaidi, M. W. Saputra, R. Marjunus, S. Sembiring, and S. Hadi (2021). The Quenching and Sonication Effect on the Mechanical Strength of Silver Nanowires Synthesized Using the Polyol Method. *Molecules*, **26**(8); 2167

Khan, M. (2018). *Silver Nanoparticles Fabrication, Characterization and Application*. British Library

Kim, H. Y., K. Kim, J. Yang, and M. K. Choi (2024). High-Resolution Intaglio Transfer Printing of Silver Nanowires for Wearable Electrophysiological Sensors. *Advanced Materials Technologies*, **9**(1); 1–8

Krishnamurthy (1977). Silver Nitrate, Pure, and Analytical Reagent. Technical Report 2214

Lakshmi, P. (2016). *The Encyclopedia of Spices and Herbs*. An Imprint of HarperCollinsPublisher

Liu, X. L., S. Han, S. B. Zhang, S. S. Zhou, N. Jiao, H. Y. Zhao, and J. Li (2020). One-Step Growth Method of Silver Nanowires in Aqueous Environment. *Materials Research Express*, **7**(9); 095001

Mamuru, S. A. and M. Happy (2018). Interrogating the Electrochemical Potential of Senna Obtusifolia Mediated Biosynthesized Silver Nanoparticles. *Journal of Nanoscience and Technology*, **4**(4); 427–430

Menamparambath, M. M., C. Muhammed Ajmal, K. Hee Kim, D. Yang, J. Roh, H. Cheol Park, C. Kwak, J. Y. Choi, and S. Baik (2015). Silver Nanowires Decorated with Silver Nanoparticles for Low-Haze Flexible Transparent Conductive Films. *Scientific Reports*, **5**; 1–3

Mozammel, M., S. K. Sardnezhaad, and E. Ahmadi (2006). Kinetics of Silver Dissolution in Nitric Acid from Ag-Au0.04-Cu0.10 and Ag-Cu0.23 Scraps. *Journal of Materials Science and Technology*, **22**(5); 696–699

Özmetin, C., M. Çopur, M. M. Kocakerim, and S. Yapici (2001). Crystallization of Silver Nitrate from Saturated Silver Nitrate Solution in Nitric Acid. *Indian Journal of Chemical Technology*, **8**(2); 112–119

Robinson, J., S. P. Munagala, A. Arjunan, N. Simpson, R. Jones, A. Baroutaji, L. T. Govindaraman, and I. Lyall (2022). Electrical Conductivity of Additively Manufactured Copper and Silver for Electrical Winding Applications. *Materials*, **15**(21); 7563

Sembiring, S., A. Riyanto, I. Firdaus, Junaidi, and R. Situmeang (2022). Structure and Properties of Silver-Silica Composite Prepared From Rice Husk Silica and Silver Nitrate. *Ceramics - Silikaty*, **66**(2); 167–177

Siddiqui, T., M. K. Zia, M. Muaz, H. Ahsan, and F. H. Khan (2023). Synthesis and Characterization of Silver Nanoparticles (AgNPs) Using Chemico-Physical Methods. *IJCA (Indonesian Journal of Chemical Analysis)*, **6**(2); 124–132

Villalpando, M., A. Saavedra-Molina, and G. Rosas (2020). A Facile Synthesis of Silver Nanowires and Their Evaluation in the Mitochondrial Membrane Potential. *Materials Science and Engineering C*, **114**; 110973

Wiley, B., Y. Sun, and Y. Xia (2005). Polyol Synthesis of Silver Nanostructures: Control of Product Morphology with Fe(II) or Fe(III) Species. *Langmuir*, **21**(18); 8077–8080

Xia, Y., Y. Xiong, B. Lim, and S. E. Skrabalak (2009). Shape-Controlled Synthesis of Metal Nanocrystals: Simple Chemistry Meets Complex Physics? *Angewandte Chemie - International Edition*, **48**(1); 60–103

Zaman, Y., M. Z. Ishaque, R. Sattar, M. M. Rehman, I. Saba, S. Kanwal, M. Akram, M. Shahzad, H. Kanwal, R. Qadir, and A. B. Siddique (2022). Antibacterial Potential of Silver Nanoparticles Synthesized Using Tri-Sodium Citrate via Controlled Exploitation of Temperature. *Digest Journal of Nanomaterials and Biostructures*, **17**(3); 979–987

Zhang, R. and M. Engholm (2018). Recent Progress on the Fabrication and Properties of Silver Nanowire-Based Transparent Electrodes. *Nanomaterials*, **8**(8); 1–17

